



University of Dundee

Blocking effects on mean ocean currents by offshore wind farm foundations

Carpenter, Jeffrey R.; Guha, Anirban

Published in:
Physical Review Fluids

DOI:
[10.1103/physrevfluids.9.103802](https://doi.org/10.1103/physrevfluids.9.103802)

Publication date:
2024

Document Version
Peer reviewed version

[Link to publication in Discovery Research Portal](#)

Citation for published version (APA):
Carpenter, J. R., & Guha, A. (2024). Blocking effects on mean ocean currents by offshore wind farm foundations. *Physical Review Fluids*, 9(10), Article 103802. <https://doi.org/10.1103/physrevfluids.9.103802>

General rights

Copyright and moral rights for the publications made accessible in Discovery Research Portal are retained by the authors and/or other copyright owners and it is a condition of accessing publications that users recognise and abide by the legal requirements associated with these rights.

Take down policy

If you believe that this document breaches copyright please contact us providing details, and we will remove access to the work immediately and investigate your claim.

1 **Blocking effects on mean ocean currents by offshore wind farm**
2 **foundations**

3 Jeffrey R. Carpenter*

4 *Institute for Coastal Ocean Dynamics,*

5 *Helmholtz-Zentrum Hereon, Geesthacht 21502, Germany*

6 Anirban Guha

7 *School of Science and Engineering,*

8 *University of Dundee, Dundee, UK*

9 (Dated: February 7, 2025)

This is the accepted manuscript version of: Carpenter, JR & Guha, A 2024, 'Blocking effects on mean ocean currents by offshore wind farm foundations', *Physical Review Fluids*, vol. 9, no. 10, 103802. <https://doi.org/10.1103/physrevfluids.9.103802>

Abstract

The continued development of shallow continental shelf regions with offshore wind farm (OWF) structures raises the question of what potential hydrodynamic impacts may be expected. One such impact is a reduction in the ocean currents that results from the additional frictional drag from the turbine foundation structures. To understand this potential ‘blocking’ effect, we construct a fluid mechanical model consisting of an idealised circular patch of OWF with increased friction. The idealised OWF is then subjected to a steady mean flow superimposed on much stronger elliptical tidal currents – a common scenario in shelf seas with OWF installations. Due to the quadratic dependence of friction on fluid velocity, the elliptical tidal currents result in a linearised friction acting on the mean flow that is no longer parallel to the mean flow. This ‘anisotropic’ friction has the effect of deflecting, in addition to reducing, the mean flow in the region of the OWF. However, it is found that a good approximation to the reduction of flow caused by OWFs can be obtained by the simplest linear, isotropic representation of the friction, i.e., a linear drag law. The flow reduction within the OWFs is found to be primarily dependent on the ratio of the increase in drag coefficient inside the farm to that of the surroundings, with weaker dependencies on the parameters describing the tidal ellipse. The magnitudes of the flow reductions in the idealised model appear to be in approximate agreement with more realistic modelling results, and are expected to capture the basic balance of the mean flow in the blocking of ocean currents by many OWFs in the North Sea, especially with increasing size in future development scenarios.

I. INTRODUCTION

In efforts to shift energy production to more carbon neutral forms, there has been a rapid expansion of offshore wind farm (OWF) development in coastal waters [1, 2]. To reach promised levels of sustainable energy production, many governments are currently planning rapid expansions of OWF resources in the near future [3]. There is therefore a pressing need to understand and quantify any potential impacts of these offshore developments on the physical oceanography of coastal seas [4–6]. These potential physical changes are expected to have cascading effects that may have the potential to alter marine productivity [7, 8] and higher trophic levels, such as fish and whale populations [4, 9].

* jeff.carpenter@hereon.de

38 Changes in the physical oceanography arising from OWFs can be expected through the
39 production of turbulent wakes in both the atmosphere [10–12] and ocean [13–15]. Although
40 important contributions to ocean currents could arise from the altered wind stress on the
41 ocean surface [12, 16], we neglect this aspect of the potential oceanographic changes to
42 focus on the changes induced by the interaction of ocean currents with the OWF foundation
43 structures. Such an interaction has been found to lead to turbulence levels that are increased
44 from the natural environment [15, 17], which cause changes to the stratification [14–16, 18,
45 19], and to mean ocean currents [19]. Little effect is expected to tidal currents (see [20], and
46 section VI).

47 This study is motivated by the finding in Christiansen et al.[19] that OWFs in the south-
48 ern North Sea are capable of altering mean (i.e. non-tidal) currents by as much as 10%
49 of existing values. We therefore, undertake an idealised theoretical study of this process
50 in order to better understand the basic physics at work. The model that we employ has
51 been first discussed in Garrett and Cummins[21], where they present an analytical study
52 that approximates the 'blocking' effects of a circular region of structures with increased
53 friction in a shallow shelf sea subject to tides. The goal of Garrett and Cummins [21] was
54 to understand feedbacks between tidal energy extraction and tidal friction. Some of these
55 solutions are outlined below in the context of understanding similar effects in offshore wind
56 farms. Presently, we extend the Garrett and Cummins [21] study by allowing for a modified
57 anisotropic friction term that results from the quadratic nature of the bottom friction in the
58 presence of strong tidal currents. We therefore examine the blocking effects of *mean* currents
59 (i.e. those resulting from averaging over many tidal cycles) by OWFs, while accounting for
60 the dominant tidal currents and how they are capable of modifying the bottom friction.

61 The paper consists of a mathematical formulation of the problem, where we outline a basic
62 derivation of the equations and boundary conditions that apply. We then find solutions for
63 two special cases: (i) perfectly circular tidal currents which leads to a linear frictional drag
64 formulation, and (ii) the limit of infinite friction within the OWF, where it can effectively
65 be replaced by a circular impenetrable boundary. Then, we solve the full problem and relate
66 it to the special cases above when examining the effects of variable tidal current parameters
67 and OWF friction levels. Finally, we apply the idealised model findings to make predictions
68 for three North Sea OWFs, and find similar blocking effects of the mean currents to the more
69 realistic modelling study of Christiansen et al. [19] for two of the OWFs, and a negligible

70 impact on the currents for the other OWF.

71 II. PROBLEM FORMULATION

72 Our model of the circulation of mean currents in shallow shelf seas consists of the shallow
 73 water equations on an f -plane, subject to quadratic friction. Mathematically this is written
 74 as

$$75 \quad \frac{\partial \vec{u}}{\partial t} + \vec{u} \cdot \vec{\nabla} \vec{u} + \vec{f} \times \vec{u} + g \vec{\nabla} h = -\frac{C_D}{H+h} |\vec{u}| \vec{u} \quad (1)$$

76 with $\vec{u} = (u, v, 0)$ the depth mean horizontal velocity on the horizontal Cartesian coordinate
 77 system $(x, y, 0)$, $\vec{f} = (0, 0, f)$ the vertical component of the Coriolis vector, g the gravitational
 78 acceleration, h the elevation of the sea surface with respect to the still water depth H , and
 79 C_D the frictional drag coefficient. We assume that variations in h are over a much larger
 80 scale than the region of interest. Then we can take the horizontal mean flow to be divergence
 81 free [21], so

$$82 \quad \vec{\nabla} \cdot \vec{u} = 0. \quad (2)$$

83 This allows us to represent the flow by a stream function, ψ , such that $\vec{u} = (\partial\psi/\partial y, -\partial\psi/\partial x)$.

84 Furthermore, we will only look for steady solutions of the above equation with the non-
 85 linear term neglected. Justification for this approximation is considered later on.

86 A. Friction of offshore wind farms

87 In this study, the current alterations of offshore wind farms are accounted for through
 88 their modification of the drag coefficient, C_D , in (1). Drag forces per unit area arising from
 89 the boundary layer that develops over the sea bed are typically represented by the drag law

$$90 \quad \vec{F} = -\rho_0 C_D^0 |\vec{u}| \vec{u}, \quad (3)$$

91 where we denote a representative water density by ρ_0 , and the sea bed drag coefficient by
 92 C_D^0 . The presence of the foundation structures give rise to an additional drag force on the
 93 currents, above that provided by the sea bed. We quantify this by the following drag law
 94 (see [14]) for the force per unit horizontal area

$$95 \quad \vec{F} = -\frac{\rho_0 C_D^t A_f}{2\ell^2} |\vec{u}| \vec{u}, \quad (4)$$

96 with the structure specific drag coefficient given by C_D^t , the frontal area of the structure
 97 by A_f , and a typical horizontal spacing of the structures represented by the distance ℓ .
 98 Although the drag force of each structure will manifest itself as a turbulent wake, we concern
 99 ourselves with the mean overall effect of the entire farm (composed of many structures) once
 100 the various individual wakes have merged. Therefore, we increase the background (sea bed)
 101 drag coefficient, C_D^0 , by the value $C_D^t A_f / (2\ell^2)$ within the OWF area to quantify the OWF
 102 effect. An important dimensionless parameter that is used to quantify this increase in
 103 friction is the friction ratio [21], $q \equiv C_D^t A_f / (2C_D^0 \ell^2)$, giving the ratio between the additional
 104 structure-induced friction, and the background. Typical values of these parameters have
 105 been tabulated for a number of OWFs in the North Sea in Table I, and a discussion is
 106 presented in section V.

107 In our estimates of the friction ratio and drag coefficients we have neglected the effects of
 108 any scour protection measures that often take the form of an irregular rock layer around the
 109 structure base. This would be expected to lead to additional friction that is not accounted
 110 for.

111 B. Friction in strong tidal flows

112 The quadratic friction term makes analytical solutions difficult. However, it is possible to
 113 simplify this term by considering a flow that is composed of two components, $\vec{u} = \vec{u}_0 + \vec{u}_1$,
 114 where \vec{u}_0 represents the relatively small and (presumed) steady mean flow, and \vec{u}_1 the larger
 115 amplitude and rapidly varying tidal currents. We assume that $|\vec{u}_0| \ll |\vec{u}_1|$; a situation that
 116 is generally true in many coastal seas, where OWFs are constructed (see Table I for typical
 117 values). We note that the nonlinear frictional drag term can then be approximated through

$$118 \frac{C_D}{H} |\vec{u}| \vec{u} \approx \mathbf{K} \vec{u}_0 \equiv \begin{bmatrix} K_{xx} & K_{xy} \\ K_{yx} & K_{yy} \end{bmatrix} \vec{u}_0 \quad (5)$$

119 following [22]. This approximation is accurate to order $O(|\vec{u}_1|/|\vec{u}_0|)$. We now define $\mathbf{K} \equiv c \mathbf{k}$,
 120 where $c = C_D/H$ so we can write

$$121 \mathbf{k} = \begin{bmatrix} k_{xx} & k_{xy} \\ k_{yx} & k_{yy} \end{bmatrix} \quad (6)$$

TABLE I. Parameter estimates for OWF foundation geometries, tidal, and mean flow currents, at three wind farms in the North Sea: BARD 1 Offshore (54.4°N, 6.0°E), Global Tech (54.5°N, 6.4°E), and the Dogger Bank group consisting of Dogger Bank A,B,C and Sophia (55°N, 2.2°E).

Parameter	Symbol (Unit)	Wind Farm		
		BARD 1	Global Tech	Dogger Bank
<i>Foundation geometry:</i>				
Frontal area	A_f (m ²)	402	560	155 – 300
Turbine spacing	ℓ (m)	866	733	2450
Drag coefficient	C_D^t (-)	1.0	1.0	1.0
Depth	H (m)	40	40	18 – 35
<i>M2 Tidal currents:</i>				
Tidal amplitude	\tilde{u} (m s ⁻¹)	0.41	0.41	0.26
Ellipse axis ratio	\tilde{b} (-)	0.11	0.15	0.29
Orientation	$\tilde{\theta}$ (°)	-14	-23	6
<i>Mean flow:</i>				
Magnitude	U (m s ⁻¹)	0.026	0.020	0.022
Direction	λ_0 (°)	45	90	127
<i>Dimensionless control parameters:</i>				
Friction ratio	q (-)	0.11	0.21	≤ 0.01
Mean/tidal current ratio	$ \vec{u}_0/\vec{u}_1 $ (-)	0.06	0.05	0.08
Nonlinearity parameter	ξ (-)	$O(1)$	$O(1)$	0.3 – 0.6
<i>Model predictions:</i>				
Reduction	(-)	0.048	0.086	< 0.01
Deflection	(°)	< 1	< 1	< 1

122 where

$$123 \quad k_{xx} = \left\langle \frac{2u_1^2 + v_1^2}{|\vec{u}_1|} \right\rangle, \quad k_{yy} = \left\langle \frac{u_1^2 + 2v_1^2}{|\vec{u}_1|} \right\rangle, \quad k_{xy} = k_{yx} = \left\langle \frac{u_1 v_1}{|\vec{u}_1|} \right\rangle \quad (7)$$

124 with the angled brackets referring to an average over a suitable period that is long compared
125 to the dominant tidal periods.

126 In practise, we will represent the tidal currents by a single tidal frequency component
127 that take the form of a tidal ellipse, and average over this tidal period. Mathematically, this

128 can be written

$$129 \quad u_1(t) = \tilde{u}[\cos(\omega t) \cos(\tilde{\theta}) - \tilde{b} \sin(\omega t) \sin(\tilde{\theta})], \quad v_1(t) = \tilde{u}[\cos(\omega t) \sin(\tilde{\theta}) + \tilde{b} \sin(\omega t) \cos(\tilde{\theta})] \quad (8)$$

130 where $0 \leq \tilde{b} \leq 1$ is the ratio of the minor to major axes of the current ellipse. It represents
 131 how elliptic the currents are, with $\tilde{b} = 0$ giving rectilinear currents, and $\tilde{b} = 1$ circular
 132 currents. Note that taking $\tilde{b} < 0$ gives a change in the ellipse rotation direction, however,
 133 the \mathbf{k} components are invariant to this change and we keep $\tilde{b} > 0$ without loss of generality.
 134 The orientation of the major axis of the ellipse is given by $\tilde{\theta}$. Using this form for the tidal
 135 currents means we can express the friction tensor components as $k_{ij} = \tilde{u}f(\tilde{b}, \tilde{\theta})$.

136 Using the tidal friction tensor form for the friction term, results in a single equation for
 137 ψ , which henceforth represents the streamfunction of the steady mean flow. The equation
 138 is derived by taking the vertical component of the curl of (1), using (5). This is expressed
 139 as $\hat{k} \cdot (\vec{\nabla} \times \mathbf{K}\vec{u}) = 0$, with \hat{k} the vertical unit vector. In terms of ψ we can expand this to

$$140 \quad L_1[\psi] + L_2[\psi] = 0 \quad (9)$$

141 where we have denoted

$$142 \quad L_1 \equiv K_{yy} \frac{\partial^2}{\partial x^2} - 2K_{xy} \frac{\partial^2}{\partial x \partial y} + K_{xx} \frac{\partial^2}{\partial y^2}. \quad (10)$$

143 and

$$144 \quad L_2 \equiv \left(\frac{\partial K_{yy}}{\partial x} - \frac{\partial K_{xy}}{\partial y} \right) \frac{\partial}{\partial x} + \left(\frac{\partial K_{xx}}{\partial y} - \frac{\partial K_{xy}}{\partial x} \right) \frac{\partial}{\partial y}. \quad (11)$$

145 **C. OWF geometry**

146 In order to facilitate the development of analytical solutions, we choose an idealised OWF
 147 geometry that is represented by a circular region of radius R , as in Garrett and Cummins
 148 [21]. The boundary of the OWF is denoted throughout by Γ . We then take the friction
 149 coefficient to have a constant background value, c_0 , and an increase to $c_0 + c_t$ within the
 150 circular OWF. This can be written mathematically as

$$151 \quad c(r) = c_0 + c_t \mathcal{H}(R - r) \quad \Rightarrow \quad \vec{\nabla} c = (-c_t \delta(R - r), 0) \quad (12)$$

152 where \mathcal{H} is the Heaviside step function and δ the Dirac delta function, and we have switched
 153 to the standard polar coordinates (r, θ) .

154 **D. Boundary conditions**

155 In the regions where the drag coefficient is constant, i.e., inside and outside of the OWF,
 156 we can write the equation for ψ as

$$157 \quad K_{yy} \frac{\partial^2 \psi}{\partial x^2} - 2K_{xy} \frac{\partial^2 \psi}{\partial x \partial y} + K_{xx} \frac{\partial^2 \psi}{\partial y^2} = 0. \quad (13)$$

158 The two solutions of (13) in these regions can then be connected by applying the jump
 159 conditions of (i) continuous streamlines, and (ii) integrating the full equation across the
 160 OWF boundary (see below and Appendix A). Note that the equation (13) remains elliptic
 161 regardless of the tidal parameters, since $K_{xy}^2 / (K_{xx} K_{yy}) < 1$ always.

162 In addition to the jump conditions, a far-field boundary condition will be applied that
 163 requires the flow to approach that of an undisturbed free stream far from the OWF. Math-
 164 ematically, this is represented as

$$165 \quad \psi(x, y) \rightarrow \text{Im}\{U e^{-i\lambda_0} z\} \quad \text{as} \quad |z| \rightarrow \infty \quad (14)$$

166 with $z \equiv x + iy$, U denoting the magnitude of the free stream flow, and λ_0 the angle that
 167 the free stream makes to the horizontal.

168 **III. ISOTROPIC TIDAL FRICTION – LINEAR DRAG**

169 This section describes the method of solution for the problem by looking first at the
 170 simplest case so that we build up to the full solution stepwise. We therefore look at the
 171 situation where the friction tensor is what we will refer to as isotropic, being proportional
 172 to the identity matrix, i.e., where $K_{xy} = 0$ and $K_{xx} = K_{yy}$. This situation occurs when the
 173 tidal currents are circular with $\tilde{b} = 1$; having no preferred orientation. This is equivalent to
 174 representing the friction by a linear drag law, as in Garrett and Cummins [21].

175 **A. Problem definition**

176 The governing equation (9) then reduces to

$$177 \quad c \nabla^2 \psi + \vec{\nabla} c \cdot \vec{\nabla} \psi = 0. \quad (15)$$

178 It is important to note that this equation, together with our chosen form for the friction
 179 coefficient, results in a singular delta function behaviour of the second term on the OWF
 180 boundary at $r = R$, whereas Laplace's equation applies everywhere else in the domain, i.e.,

$$181 \quad \nabla^2 \psi = 0 \quad \text{for } r \neq R. \quad (16)$$

182 To connect the two solutions in the regions inside and outside the OWF we apply the jump
 183 conditions.

184 The first of these jump conditions corresponds to the continuity of streamlines, i.e.,

$$185 \quad \llbracket \psi \rrbracket_R = 0, \quad (17)$$

186 where we use the notation that $\llbracket f(x) \rrbracket_X \equiv f(X^+) - f(X^-)$. The second jump condition is
 187 described and derived in the appendix, and can be stated as

$$188 \quad \llbracket c\psi_r \rrbracket_R = 0. \quad (18)$$

189 Here, and henceforth, all subscripts on ψ denote partial derivatives.

190 It will be advantageous to use the complex potential function to derive solutions. This is
 191 defined as

$$192 \quad \Omega(z) \equiv \Phi(x, y) + i\psi(x, y) \quad (19)$$

193 a function of the complex variable $z \equiv x + iy$. We will be concerned exclusively with the
 194 stream function (opposed to Φ), obtained through $\psi = \text{Im}\{\Omega\}$. Using the results of complex
 195 variable theory we can also relate Ω to the velocity through

$$196 \quad \frac{d\Omega}{dz} = \psi_y + i\psi_x = u - iv. \quad (20)$$

197 **B. Solution**

198 We will immediately write a general solution to the problem of the following form

$$199 \quad \Omega(z) = Az + \begin{cases} \tau z + R^2 \bar{\tau}/z & , z\bar{z} > R^2 \\ B & , z\bar{z} < R^2 \end{cases} \quad (21)$$

200 where A, B, τ are arbitrary complex constants to be determined by applying the jump and
 201 boundary conditions, and the overbar represents a complex conjugate.

202 First, we require that the streamlines are continuous across the OWF boundary at $r = R$
 203 and find

$$204 \quad \llbracket \Omega \rrbracket_R = R(\tau e^{i\theta} + \overline{\tau e^{i\theta}}) - B, \quad (22)$$

205 with $z = R e^{i\theta}$. This shows that when B is taken to be real there is no jump in ψ across the
 206 boundary. Next, we require that the flow be uniform with velocity U , and at an angle of λ_0
 207 to the horizontal, far from the OWF. This is written mathematically as

$$208 \quad \Omega \rightarrow U e^{-i\lambda_0} z \quad \text{for} \quad |z| \rightarrow \infty. \quad (23)$$

209 Applying this condition to the solution in (21) gives an expression for A ,

$$210 \quad (A + \tau)z = U e^{-i\lambda_0} z \quad \Rightarrow \quad A = U e^{-i\lambda_0} - \tau. \quad (24)$$

211 Finally, we can solve for the last remaining constant, τ , by applying the final jump condition.

212 We do this by noting that the radial derivative of ψ can be expressed as

$$213 \quad \psi_r = \text{Im} \left(e^{i\theta} \frac{d\Omega}{dz} \right) \quad (25)$$

214 so that the jump condition can be found using

$$215 \quad \frac{d\Omega}{dz} = U e^{-i\lambda_0} - \begin{cases} R^2 \bar{\tau} / z^2 & , z\bar{z} > R^2 \\ \tau & , z\bar{z} < R^2 \end{cases} \quad (26)$$

216 We can therefore write

$$217 \quad e^{i\theta} \llbracket c \, d\Omega/dz \rrbracket_R = (1 + q)\tau e^{i\theta} - \overline{\tau e^{i\theta}} - q U e^{-i\lambda_0} e^{i\theta} \quad (27)$$

218 where we have defined the friction ratio $q \equiv c_t/c_0$. After taking the imaginary component
 219 of this and setting it to zero we can solve for τ as

$$220 \quad \tau = \frac{q}{2 + q} U e^{-i\lambda_0}. \quad (28)$$

221 The full solution can then be written as follows

$$222 \quad \Omega(z) = U e^{-i\lambda_0} \cdot \begin{cases} z + \frac{q}{2+q} e^{i2\lambda_0} R^2 / z & , z\bar{z} > R^2 \\ \frac{2}{2+q} z + B & , z\bar{z} < R^2 \end{cases} \quad (29)$$

223 with $\psi(x, y) = \text{Im}\{\Omega\}$. Furthermore, the velocities of this solution can be easily computed
 224 through $u = \text{Re}\{d\Omega/dz\}$ and $v = -\text{Im}\{d\Omega/dz\}$.

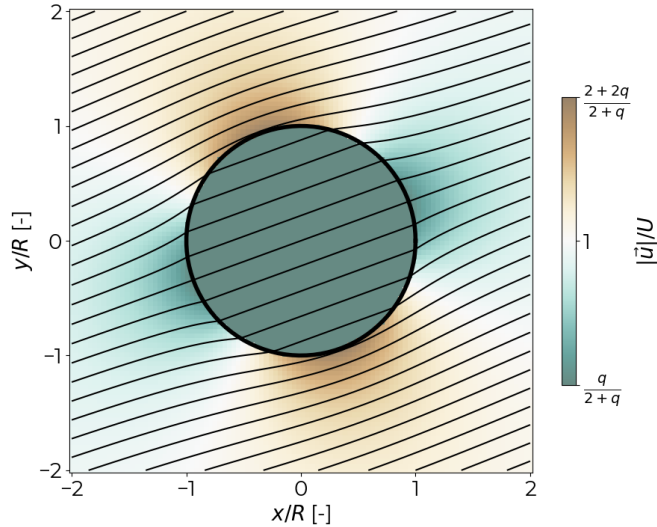


FIG. 1. Solution of the case of linear friction for the blocking effects in an OWF area ($r < R$) with boundary delineated by the thick black line. The lines show contours of the stream function. The ratio of the linear drag coefficients in this example is $q = c_t/c_0 = 3/4$ and the far-field flow has $\lambda_0 = 20^\circ$. The colours show the magnitude of the velocity relative to the free stream, i.e., $|\vec{u}|/U$.

225 There are some interesting aspects of this solution that we now discuss. First, a solution
 226 is plotted in figure 1 for the value of $q = 3/4$, a value significantly larger than typical
 227 OWF conditions (see Table I) which we have chosen for illustrative purposes. It shows the
 228 streamlines of the flow diverging as they approach the OWF area and converging again
 229 symmetrically downstream.

230 We formulate the reduction in currents within the OWF by

$$231 \quad \text{Reduction} \equiv 1 - \frac{\sqrt{u^2 + v^2}}{U}, \quad (30)$$

232 for $r < R$. This definition allows for values between zero and unity that correspond to no
 233 reduction and complete blocking, respectively. We find that this can be expressed through
 234 a function of the friction ratio as

$$235 \quad \text{Reduction} = \frac{q}{2 + q}. \quad (31)$$

236 Note that these values are independent of the size R , of the OWF. They also have the
 237 expected limits: as $q \rightarrow 0$ there is no reduction of the currents, whereas for $q \rightarrow \infty$ there is
 238 a complete blocking of the flow with reductions of unity.

239 In addition to the current reduction within the OWF region, there is also an increase
 240 in current speed as the flow passes around the OWF (figure 1). The magnitude of this
 241 increase is greatest on the boundary of the OWF that is perpendicular to the free stream
 242 flow direction (i.e., at locations of $z = Re^{i(\lambda_0 \pm \pi/2)}$). The increase can be quantified to be
 243 equal in magnitude to the reduction, with the maximum and minimum velocities found to
 244 be $|\vec{u}|_{\max, \min}/U = 1 \pm q/(2 + q)$.

245 The solution exhibits some unrealistic features that are a result of our simplifying as-
 246 sumptions. Most notably, the currents are found to be entirely horizontal and constant
 247 within the farm. This generally results in a jump in velocity across the farm boundary. In
 248 reality this sudden change will be spread out over a transition region that is set by the wakes
 249 of the individual structures.

250 IV. ANISOTROPIC TIDAL FRICTION

251 The full anisotropic tidal friction tensor is now used in finding a solution for mean flows
 252 with friction affected by general elliptic tidal currents. The solutions will then, generally
 253 depend on the additional tidal parameters describing the orientation ($\tilde{\theta}$) and degree of el-
 254 lipticity (\tilde{b}).

255 A. Solution method by coordinate transformations

256 The approach that we take to obtain the solution of (9-12, 14) is through a series of three
 257 coordinate transformations. These are summarised in figure 2 and described in turn below.

258 1. The first coordinate transformation is designed to transform the governing equation
 259 (13), in the complex $z \equiv x + iy$ plane, into the Laplace equation in the $\xi \equiv \zeta + i\eta$
 260 plane. This transformation is given by

$$261 \quad \xi = bx + i(ax + y) \quad \text{with inverse} \quad z = \zeta/b + i(\eta - \frac{a}{b}\zeta) \quad (32)$$

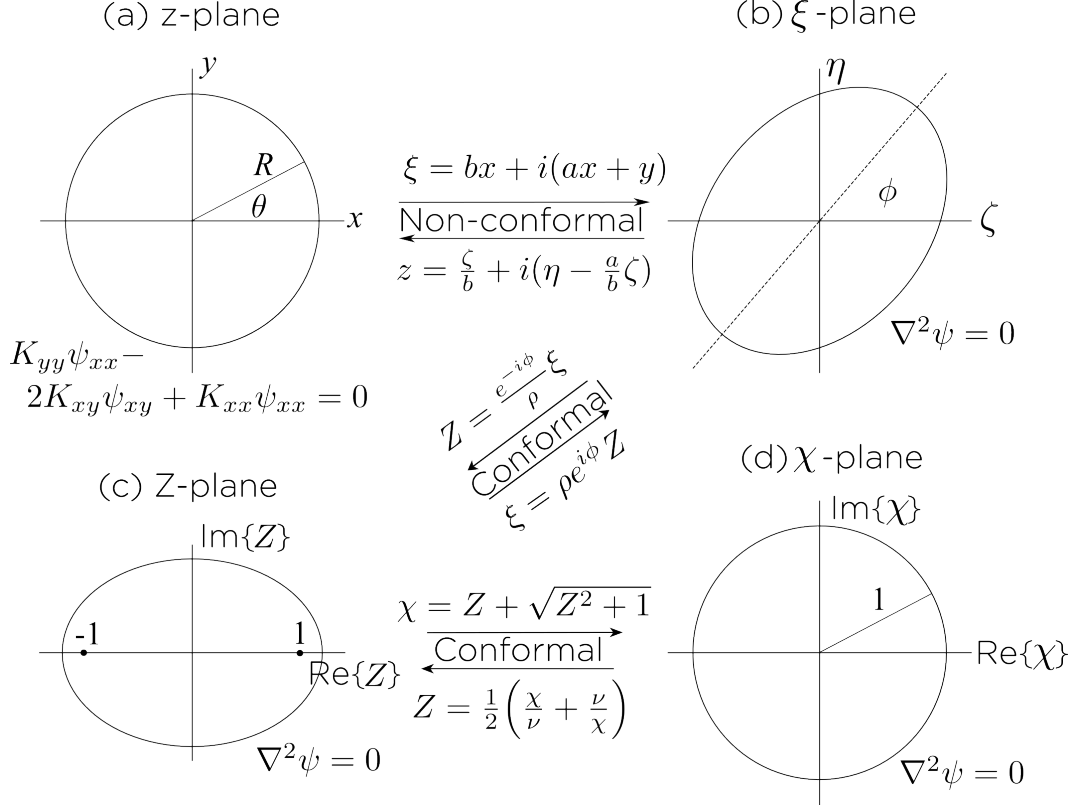


FIG. 2. Illustration of the sequence of transformations used in the solution of the anisotropic friction cases. Important parameters and scales are also shown, along with the governing equation of ψ in each domain away from the OWF boundary.

where

$$a \equiv K_{xy}/K_{yy} \quad \text{and} \quad b \equiv \left(\frac{K_{xx}K_{yy} - K_{xy}^2}{K_{yy}^2} \right)^{1/2}. \quad (33)$$

It can be written in terms of complex variables as

$$\xi = \left(\frac{b+1}{2} + i\frac{a}{2} \right) z + \left(\frac{b-1}{2} + i\frac{a}{2} \right) \bar{z} \equiv \gamma_+ e^{i\alpha} z + \gamma_- e^{i\alpha} \bar{z} \quad (34)$$

with inverse transformation of

$$z = \left(\frac{1+b}{2b} - i\frac{a}{2b} \right) \xi + \left(\frac{1-b}{2b} - i\frac{a}{2b} \right) \bar{\xi} = \frac{1}{b} \left(\gamma_+ e^{-i\alpha} \xi - \gamma_- e^{i\alpha} \bar{\xi} \right). \quad (35)$$

It may be verified that this coordinate system transforms (13) into Laplace's equation in the ξ -plane, i.e., $\psi_{\zeta\zeta} + \psi_{\eta\eta} = 0$. We note that this transformation is not conformal.

The boundary of a circular OWF with radius R in the z -plane is transformed into a tilted ellipse in the ξ -plane. With the circle parameterised by $z = Re^{i\theta}$ this ellipse has

the equation

$$\xi(\theta) = Rb \cos \theta + iR(a \cos \theta + \sin \theta) \quad (36)$$

$$= R\left(\frac{b+1}{2} + i\frac{a}{2}\right)e^{i\theta} + R\left(\frac{b-1}{2} + i\frac{a}{2}\right)e^{-i\theta} \quad (37)$$

$$= R\gamma_+ e^{i(\theta+\alpha_+)} + R\gamma_- e^{-i(\theta-\alpha_-)} \quad (38)$$

270 where we have defined $2\gamma_{\pm} \equiv (a^2 + b^2 \pm 2b + 1)^{1/2}$, and have also $\tan \alpha_{\pm} \equiv a/(b \pm 1)$.

271 2. The second coordinate transformation is chosen as a rotation and scaling of the ellipse
272 to place its focii in the Z -plane at $Z = \pm 1$. It is given by

$$273 \quad Z = \frac{e^{-i\phi}}{\rho} \xi, \quad (39)$$

274 with coefficients of

$$275 \quad \tan(2\phi) = \frac{2ab}{b^2 - a^2 - 1} \quad \text{and} \quad \rho = R(A'^{-1} - C'^{-1}) \quad (40)$$

276 with

$$277 \quad A' = \frac{1+a^2}{b^2} \cos^2(\phi) - \frac{a}{b} \sin(2\phi) + \sin^2(\phi), \quad C' = \frac{1+a^2}{b^2} \sin^2(\phi) + \frac{a}{b} \sin(2\phi) + \cos^2(\phi). \quad (41)$$

Note that because this transformation is conformal Laplace's equation must be satisfied in the Z -plane. The ellipse has the equation

$$Z(\theta) = \frac{R}{\rho} e^{-i\phi} [b \cos \theta + i(a \cos \theta + \sin \theta)] \quad (42)$$

$$= \frac{R}{\rho} [\gamma_+ e^{i(\theta+\beta)} + \gamma_- e^{-i(\theta+\beta)}] \quad (43)$$

278 in the complex Z -plane, where $2\beta \equiv \alpha_+ - \alpha_-$, and $2\phi = \alpha_+ + \alpha_-$. It is possible to
279 show that $\beta = -\tilde{\theta}$, i.e., the negative of the orientation of the major axis of the tidal
280 currents (see Appendix for derivation). The Z -plane ellipse can be seen to have major
281 and minor axes given by $2\frac{R}{\rho}(\gamma_+ + \gamma_-)$ and $2\frac{R}{\rho}(\gamma_+ - \gamma_-)$, respectively.

282 3. The final coordinate transformation takes the ellipse in the Z -plane to the unit circle
283 in the χ -plane via

$$284 \quad \chi = \nu(Z + \sqrt{Z^2 - 1}) \quad (44)$$

285 with

$$286 \quad \nu = \frac{R}{\rho\sqrt{A'}} - \sqrt{\frac{R^2}{\rho^2 A'} - 1}. \quad (45)$$

287 It is also conformal so that the stream function satisfies the Laplace equation in the
 288 χ -plane. Care must be taken in this transform to choose the correct branch cuts in
 289 the square root term. The branch cut must be placed on the line between $Z = \pm 1$.
 290 The inverse transform is given by

$$291 \quad Z = \frac{1}{2} \left(\frac{\chi}{\nu} + \frac{\nu}{\chi} \right). \quad (46)$$

292 Relationships between ν and other parameters can be derived by substituting $\chi(\theta - \tilde{\theta})$
 293 into the above equation for Z and equating the major and minor axes lengths to give
 294 $2\frac{R}{\rho}(\gamma_+ \pm \gamma_-) = \nu \pm \nu^{-1}$. For example, we can find that $2\frac{R}{\rho}\gamma_+ = \nu$ and $2\frac{R}{\rho}\gamma_- = \nu^{-1}$.

295 Now that these transformations are in place we can specify the solution for Laplace's
 296 equation in the χ -plane and then perform the inverse transformations to recover the solution
 297 in the original z -plane.

298 B. Solution for infinite q

299 This special case consists of the limit as $q \rightarrow \infty$ so that the circular OWF can be treated
 300 as a solid object. There is only one solution that applies outside the OWF area, and one
 301 boundary condition needed on the OWF boundary, namely that it must be a streamline,
 302 i.e., $\psi = 0$ on $r = R$.

303 The solution for flow around a unit circular cylinder can be expressed in the χ -plane as

$$304 \quad \Omega(\chi) = \tau\chi + \frac{\bar{\tau}}{\chi}, \quad (47)$$

305 for some appropriately chosen complex constant τ . Notice that on the unit circle we have
 306 $\chi\bar{\chi} = 1$ and Ω becomes the sum of two complex conjugate terms. This shows that the unit
 307 circle is the $\psi = 0$ streamline, and it can be confirmed that this boundary condition is also
 308 satisfied in the z -plane.

309 The final boundary condition is that the correct far-field flow is obtained. To do this, we
 310 look at how the uniform flow in the z -plane can be transformed to a condition in the χ -plane.
 311 Given the general uniform flow of $\Omega(x, y) = Ue^{-i\lambda_0}z$, we can write this in the ξ -plane as

$$312 \quad \Omega(\zeta, \eta) = \frac{U}{b}e^{-i\lambda_0}[\zeta + i(b\eta - a\zeta)]. \quad (48)$$

313 However, it can be seen that this complex potential cannot be written as a function of ξ
 314 only, i.e., we must write $\Omega = \Omega(\xi, \bar{\xi})$ since the transformation between the z - and ξ -planes
 315 is not conformal. To avoid use of the conjugate in the conformal transformations to follow,
 316 we express the complex potential in the ξ -plane in terms of an “equivalent” potential

$$317 \quad \Omega^*(\xi) = U\gamma e^{-i\lambda_1}\xi, \quad (49)$$

318 defined such that the imaginary (stream function) part gives the correct far-field flow upon
 319 transformation back to the z -plane. It can be shown that

$$320 \quad \gamma = [(a \cos \lambda_0 + \sin \lambda_0)^2 + (b \cos \lambda_0)^2]^{1/2}/b \quad \text{and} \quad \tan(\lambda_1) = \frac{a \cos \lambda_0 + \sin \lambda_0}{b \cos \lambda_0}. \quad (50)$$

321 It is now straight forward to match this uniform flow in the far-field with a condition in
 322 the χ -plane; as $|z| \rightarrow \infty$ we have also all of $|\xi|, |Z|, |\chi| \rightarrow \infty$, so

$$323 \quad \xi \rightarrow \frac{\rho}{2\nu} e^{i\phi} \chi \quad \Rightarrow \quad \Omega^* \rightarrow \frac{U\gamma\rho}{2\nu} e^{i(\phi-\lambda_1)} \chi. \quad (51)$$

324 We can therefore equate the coefficient of the first (far-field) term of (47) with (49,51) to
 325 give

$$326 \quad \tau = \frac{U\gamma\rho}{2\nu} e^{i(\phi-\lambda_1)}, \quad (52)$$

327 and a full solution of

$$328 \quad \Omega(\chi) = \frac{U\rho\gamma}{2\nu} \left[\chi e^{-i(\lambda_1-\phi)} + \frac{e^{i(\lambda_1-\phi)}}{\chi} \right]. \quad (53)$$

329 The imaginary part of this solution, giving the streamlines, is plotted in Fig. 3 for a
 330 specific example. Note that we have also included the field inside the OWF, which in
 331 this case of infinite friction is not a part of the solution domain. It is included only for
 332 mathematical insight since it shows the position of the branch cut.

333 The solution in Fig. 3 shows that the symmetry of the classical flow around a cylinder
 334 is broken with the introduction of the anisotropic friction tensor. This is best manifest
 335 through the shifting of the stagnation points on the cylinder surface through the angle θ_{sp} .
 336 By setting $d\Omega/d\chi = 0$ on the surface of the cylinder, we can solve for the locations of the
 337 stagnation points as $\theta_{\text{sp}} = \lambda_1 - \phi + \tilde{\theta}$ with $\pm\pi$ radians added to this to get the second
 338 stagnation point. The stagnation point locations are a function only of the tidal ellipse
 339 parameters $\tilde{b}, \tilde{\theta}$, and Fig. 4 shows how they change the value of θ_{sp} : the more rectilinear
 340 the tidal currents (i.e. lower \tilde{b}), and the closer to 50° the ellipse orientation (for low \tilde{b}), the
 341 larger the stagnation point angle. However, they do not reach larger than $\pm 10^\circ$ from the
 342 far-field current direction.

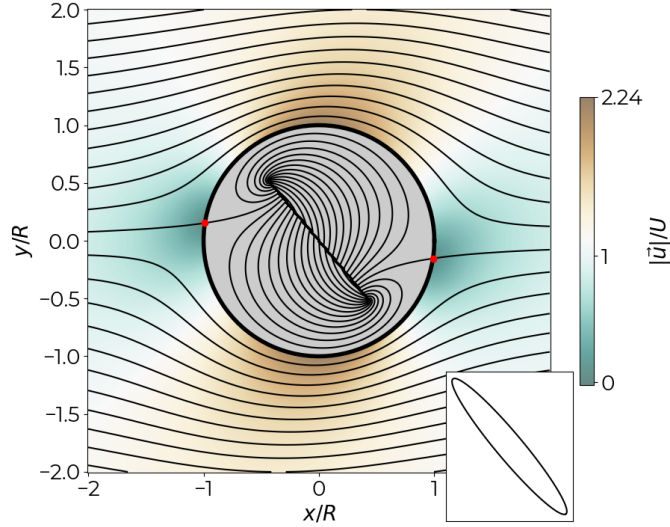


FIG. 3. Streamlines of flow past a circular OWF in the limit of infinite friction, i.e., $q \rightarrow \infty$. Streamlines within the OWF region are not part of the physical domain, and are only plotted for mathematical insight. The tidal current ellipse is plotted in the lower right inset panel with parameters of $\tilde{b} = 0.15$, $\tilde{\theta} = 60^\circ$, and $\lambda_0 = 0^\circ$. Stagnation points on the cylinder are shown as red dots with colours representing the velocity magnitude as in figure 1.

343 C. Anisotropic tidal friction – the full problem

344 Similar to our approach in the last two subsections, here we apply the same coordinate
 345 transformations and propose a trial solution of a similar form, i.e. we let

$$346 \quad \Omega = AZ + \begin{cases} \tau\chi + \bar{\tau}/\chi & , \chi\bar{\chi} > 1 \\ B & , \chi\bar{\chi} < 1 \end{cases}, \quad (54)$$

347 with A, B, τ complex constants. We also write this trial solution as $\Omega = \Omega_0(Z) + \Omega_1(\chi)$
 348 with $\Omega_0 = AZ$ defined throughout the domain, and Ω_1 (the final term in Eq 54) defined
 349 differently inside and outside the OWF area. The $\Omega_0(Z)$ part is not explicitly written in
 350 terms of χ to avoid an unnecessary singularity in the χ -plane [23]. To arrive at a solution
 351 we now apply each of the jump and boundary conditions to solve for the constants.

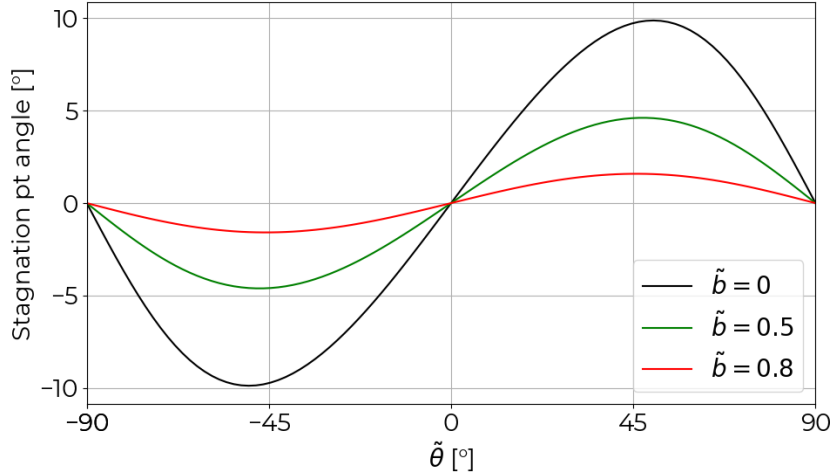


FIG. 4. Angle of the stagnation points, θ_{sp} , as a function of the tidal ellipse parameters.

352 *Jump condition 1 – Continuous streamlines*

353 The jump condition that requires continuous streamlines is easily fulfilled if we choose B
 354 to be real, since on the boundary $\chi\bar{\chi} = 1$ and inside and outside the OWF boundary Ω_1 has
 355 vanishing imaginary component. For simplicity we set $B = 0$.

356 *The far-field boundary condition*

357 In applying the far-field boundary condition from (51) to our trial solution (54) we are
 358 able to solve for A in terms of τ as

359
$$A = U\gamma\rho e^{i(\phi-\lambda_1)} - 2\nu\tau. \quad (55)$$

360 It can be seen that the second term above is chosen to exactly cancel the far-field contribution
 361 of $\Omega_1(\chi)$, with the first term then providing the correct “equivalent” potential to result in
 362 the required far-field flow (exactly as in the linear drag case).

363 *Jump condition 2*

364 The final coefficient τ , can be determined from the second jump condition. It is helpful
 365 to split the solution for ψ into two components associated with the two terms of $\Omega = \Omega_0 + \Omega_1$

366 so that $\psi = \psi^0 + \psi^1$, with ψ^1 being valid outside the OWF region only. This can then be
 367 substituted into the jump condition found in the appendix of

$$368 \quad m \left[[c\psi_r] \right]_{r=R} - \frac{nc_t}{R} \psi_\theta \Big|_{r=R} = 0, \quad (56)$$

369 where $m \equiv k_{yy} \cos^2 \theta - 2k_{xy} \sin \theta \cos \theta + k_{xx} \sin^2 \theta$ and $n \equiv (k_{xx} - k_{yy}) \sin \theta \cos \theta + k_{xy} (\sin^2 \theta -$
 370 $\cos^2 \theta)$. It is possible to simplify the jump condition above to

$$371 \quad m\psi_r^1|_{r=R} = q[\psi_x^0(m \cos \theta - n \sin \theta) + \psi_y^0(m \sin \theta + n \cos \theta)], \quad (57)$$

372 and to substitute into ψ on both sides using the trial solution in (54). The radial gradient
 373 of ψ^1 on the left hand side can be written as

$$374 \quad \psi_r = \cos \theta \psi_x + \sin \theta \psi_y = b \cos \theta \psi_\zeta + (a \cos \theta + \sin \theta) \psi_\eta. \quad (58)$$

375 This can then be combined with expressions for the gradients from the chain rule

$$376 \quad \frac{d\Omega_1}{d\xi} = \psi_\eta + i\psi_\zeta = \frac{dZ}{d\xi} \frac{d\chi}{dZ} \frac{d\Omega_1}{d\chi}, \quad (59)$$

377 where each term can be calculated from the transformations and the trial solution as

$$378 \quad \frac{dZ}{d\xi} = \frac{e^{-i\phi}}{\rho}, \quad \frac{d\chi}{dZ} = \frac{2\nu\chi^2}{\chi^2 - \nu^2}, \quad \frac{d\Omega_1}{d\chi} = \tau - \frac{\bar{\tau}}{\chi^2}. \quad (60)$$

379 Here we have expressed everything in terms of χ , and can write as

$$380 \quad \frac{d\Omega_1}{d\xi} = \frac{2\nu}{\rho e^{i\phi}} \cdot \frac{\tau\chi^2 - \bar{\tau}}{\chi^2 - \nu^2}, \quad (61)$$

381 with the OWF boundary given in the χ -plane by the parametric equation $\chi(\theta) = e^{i(\theta - \bar{\theta})}$.

382 Unfortunately, we were not able to find a manageable closed form analytical solution to
 383 the jump condition equation (57-61), and have relied on a numerical solution for the results
 384 presented in the following. Details of the solution method are described in Appendix C.

385 *Results*

386 An example of the streamlines resulting from the above solution is shown in figure 5.
 387 There are two general features of the solution that are worth noting: (i) the reduction in
 388 current strength throughout the OWF, and (ii) a slight deflection of the current direction

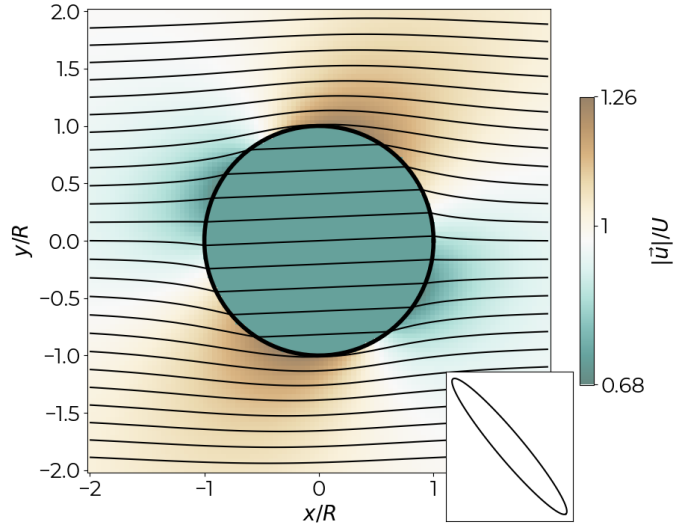


FIG. 5. Streamlines of flow past a circular OWF with the full anisotropic friction. Parameter values correspond to $q = 3/4$, $\tilde{\theta} = -50^\circ$, $\tilde{b} = 0.15$, and $\lambda_0 = 0^\circ$. The tidal ellipse is shown in the lower right inset. The flow within the OWF shows a reduction in current of 0.27 and a deflection of 2.1° .

389 within the OWF. The reduction was defined in (30) above, and the deflection is defined
 390 mathematically by

$$391 \quad \text{Deflection} \equiv \tan^{-1} \left(\frac{v}{u} \right) - \lambda_0 \quad (62)$$

392 where $\vec{u} = (u, v) = (\psi_y, -\psi_x)$ is the flow within the OWF region, $r < R$. By first fixing
 393 the parameters describing the tidal ellipse ($\tilde{b}, \tilde{\theta}$), and the far-field flow angle ($\lambda_0 = 0$), both
 394 the reduction and deflection of the flow within the OWF area are plotted as a function of
 395 the friction coefficient, q , in figure 6. It can be seen that the reduction in current strength
 396 follows the linear drag solution of $q/(2+q)$, described in section III, very closely (figure 6a,
 397 dashed line). This result also holds when other values of \tilde{b} and $\tilde{\theta}$ are chosen. As expected,
 398 the reduction in currents approaches unity as $q \rightarrow \infty$, and vanishes as $q \rightarrow 0$.

399 An additional aspect of the solution that arises when anisotropic friction is used, is the
 400 deflection of the currents within, and around, the OWF. This was first seen in the infinite

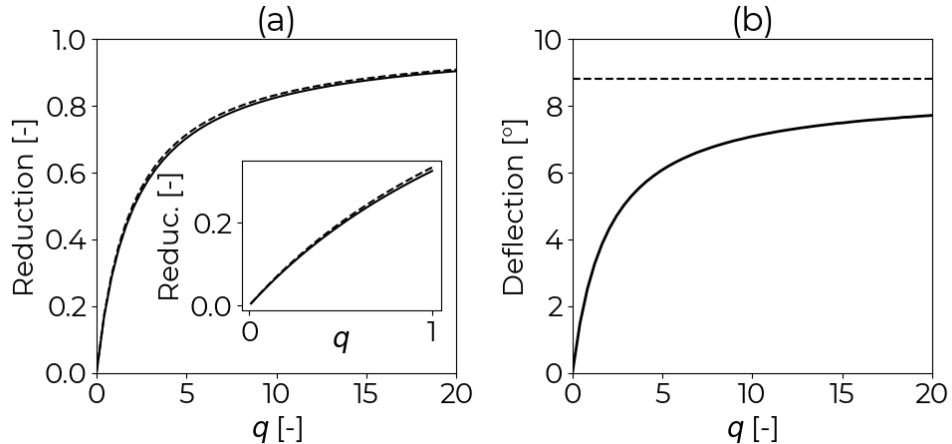


FIG. 6. The reduction (a) and deflection (b) of the flow within the OWF as a function of the friction coefficient, q . The dashed line in (a) is the linear friction result for the reduction in current strength given by $q/(2+q)$. The inset in (a) shows the reduction in the OWF-relevant range of q . The dashed line in (b) represents the stagnation point angle at infinite friction. Other parameters taken for these plots are $\tilde{b} = 0.15$, $\tilde{\theta} = -50^\circ$, $\lambda_0 = 0^\circ$.

401 friction case in section IV B for $q \rightarrow \infty$, where a shifting of the position of the stagnation
 402 points was found. As q increases in figure 6(b) we see the deflection of the flow within the
 403 OWF being bounded by this stagnation point value.

404 The dependence of the current reduction and deflection on the orientation of the tidal
 405 ellipse is plotted in figure 7. Here we have fixed $\tilde{b} = 0$, giving rectilinear tidal currents for
 406 which the largest deviations from the linear drag case are seen. Since the current reduction
 407 follows the $q/(2+q)$ scaling so closely, we have normalised the reduction by this amount to
 408 look at variation around this level in figure 7(a). The results show that $\tilde{\theta}$ can cause departures
 409 from the $q/(2+q)$ result by more than $\pm 10\%$, with the largest magnitudes found at the
 410 lowest OWF friction (q) levels, and at tidal current orientations that are parrallel (highest
 411 reduction) and perpendicular (smallest reduction) to the mean flow. Little deviation from
 412 the linear drag scaling result are seen when the tidal current orientation is at 45° to the mean
 413 flow (figure 7a). On the other hand, the deflection shows a maximum close to orientations
 414 of 45° , with trends of increasing deflection for increased friction ratio (figure 7b).

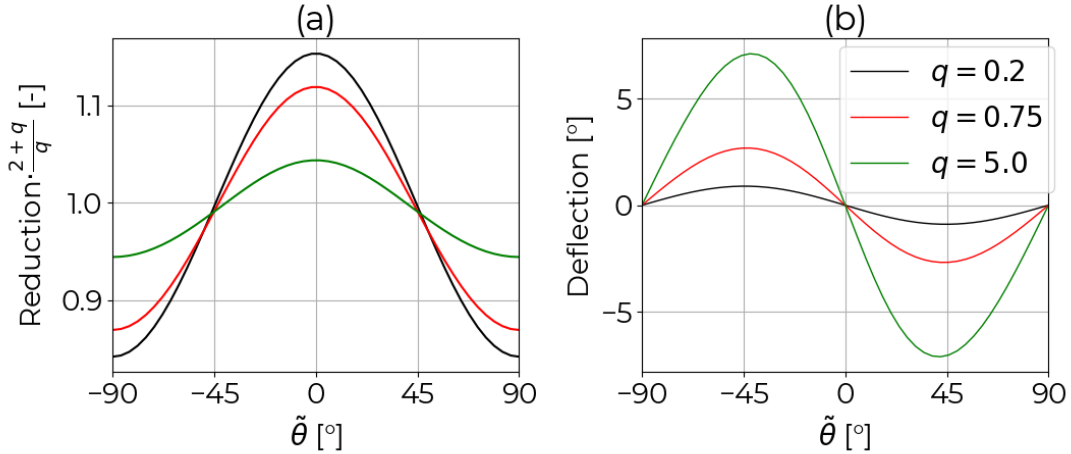


FIG. 7. The reduction (a) and deflection (b) of the flow within the OWF as a function of the tidal ellipse orientation, $\tilde{\theta}$. The reduction values in (a) have been normalised by the linear drag scaling of $q/(q + 2)$. For all curves $\tilde{b} = 0$.

415 V. APPLICATION TO OWFS IN THE NORTH SEA

416 In this section, we tabulate typical parameters for three OWFs in the North Sea, and
 417 apply the solution described above to arrive at expected values of current reductions and
 418 deflections.

419 The friction ratios of typical OWFs can be expressed in terms of tabulated values, as in
 420 section II A, through

$$421 \quad q \equiv \frac{c_t}{c_0} = \frac{C_D^t}{2C_D^0} \cdot \frac{A_f}{\ell^2}. \quad (63)$$

422 We find it helpful to think of q as being composed of the product of two terms (as formatted
 423 in equation 63 above). The first being a simple ratio of drag coefficients for the OWF
 424 foundation structures and the flat sea bed, with much higher drag coefficients associated
 425 with the separated wakes of the cylindrical foundation structures than the bottom boundary
 426 layer of the sea bed. However, this larger structure drag coefficient factor is outweighed by
 427 the second factor, the ratio of the structure frontal area to the area of sea bed around a
 428 foundation structure (ℓ^2). The resulting values of q are then typically well below unity.
 429 For the BARD 1 and Global Tech OWFs in the southern North Sea, Carpenter et al. [14]
 430 have estimated these areas and drag coefficients, and using their values we find $q = 0.11$ for

431 BARD 1 and $q = 0.21$ for Global Tech (Table I). Very different friction ratios can be found
 432 in the Dogger Bank group of OWFs, where a relatively wide spacing of the monopile turbine
 433 foundations ($\ell \approx 2.4$ km) leads to a very low $q = O(0.01)$. A summary of the relevant
 434 parameter estimates for the Dogger Bank OWFs (Dogger Bank A, B, C, and Sophia, which
 435 are still being installed at this time), which we group together, are presented in Table I.

436 The tidal currents and mean flows at the OWF sites are derived from regional simulations
 437 designed to study the effects of OWFs on North Sea oceanography, as described in Chris-
 438 tiansen et al. [12, 19]. They have currents that are dominated by the M2 tidal component
 439 with values that characterise the tidal ellipse, and the mean flow shown in Table I. All other
 440 tidal components have been neglected for simplicity, but can easily be accounted for in the
 441 computation of the tidal friction tensor. From the parameters in Table I we can verify the
 442 assumption that the tidal currents are much larger than the mean flow, i.e., $U/\tilde{u} < O(0.1)$
 443 at all OWFs.

444 With the parameters listed in Table I we are able to make estimates of the reduction and
 445 deflection of the mean currents in an idealised OWF with similar friction, tidal, and mean
 446 flow parameters as those in Table I, but with our idealised circular geometry. Application of
 447 the model solution described in section IV C above results in mean flow current reductions
 448 of 0.048 and 0.086 in BARD and Global Tech, respectively, and deflections of less than one
 449 degree (see ‘Model predictions’ section of Table I). These estimates of the current reductions
 450 are within the range reported in [19], who use a drag-based increase of the bottom stress
 451 and turbulence production in a realistic simulation of OWFs in the North Sea. The current
 452 blocking effects of the Dogger Bank OWF however, are predicted to be negligible. This is
 453 due to the one order of magnitude smaller friction ratio that comes with the significantly
 454 larger foundation structure spacing, ℓ .

455 VI. DISCUSSION

456 Our derivation of the solution for blocking effects within, and around, OWFs has made
 457 some simplifying assumptions that are worth discussing in more detail. The first such
 458 assumption was the neglect of the nonlinear advection terms in (1). Following Garrett
 459 and Cummins [21], we evaluate the importance of the nonlinear terms through an order of
 460 magnitude analysis, comparing them to the friction term. Noting that the nonlinear terms

461 are expected to scale with the tidal velocity, \tilde{u} , and the length scale of the OWF, R , we find
 462 $\vec{u} \cdot \nabla \vec{u} \sim \tilde{u}^2/R$. Similarly, the friction term is $C_D^0 \tilde{u}^2/H$. Taking the ratio of these two terms,
 463 for our assumption to hold we require the dimensionless number

$$464 \quad \xi \equiv \frac{H}{C_D^0 R} \ll 1. \quad (64)$$

465 Substituting in for each quantity in ξ for the BARD and Global Tech OWFs from Table I,
 466 and choosing a representative $R = 10$ km, gives the estimate of $\xi = O(1)$. Therefore, we
 467 expect that the nonlinear terms could play a role in the dynamics of these OWFs at their
 468 current sizes. As the size of OWFs grows in the future, this will have the effect of reducing
 469 ξ to limit the nonlinear effects. In the Dogger Bank OWF we find lower values in the range
 470 of $\xi = 0.3 - 0.6$.

471 Even if we considered only cases with $\xi \ll 1$, the neglect of the nonlinear terms is not
 472 universally valid throughout the solution domain. In particular, we have assumed above
 473 that the length scale of variability in the solution is R , whereas the actual solution shows
 474 rapid variability at the OWF boundary (figure 5). In these regions a full solution would give
 475 a smooth transition across the boundary.

476 Another simplifying assumption that was made in deriving the solution was to neglect
 477 any feedbacks between the increased friction of the OWF and the tidal currents. This is also
 478 expected to be accurate if the friction term is not of leading order in the balance of the tidal
 479 currents. We assess this by comparing the magnitude of the unsteady term for an M2 tidal
 480 forcing, $\partial \vec{u} / \partial t \sim \tilde{u} \omega_{M2}$, with ω_{M2} the angular frequency of the M2 tide, to the friction term
 481 of the tidal currents, $C_D^0 \tilde{u}^2/H$. Using the typical values listed above, we find the unsteady
 482 term to be a factor of approximately 5 larger. We therefore expect that the introduction of
 483 increased friction from the OWFs does not lead to large changes in tidal currents, as found
 484 in Cazenave et al. [20].

485 VII. CONCLUSIONS

486 An idealised model has been developed of the process by which the increased frictional
 487 drag of offshore wind farms (OWFs) creates a ‘blocking’ of mean ocean currents. This
 488 was done by extending the previous work of Garrett and Cummins [21] to allow for a
 489 modified ‘anisotropic’ friction that arises from the quadratic drag law in the presence of

490 strong elliptical tidal currents. The modification requires that a series of transformations be
491 made to convert the elliptical partial differential equation to Laplace’s equation, and into a
492 circular geometry that can be solved with known solutions.

493 The results predict that for typical values of OWF foundation structures in the southern
494 North Sea, the reduction of mean current magnitudes within the farms can be up to ap-
495 proximately 10%, depending on the relatively uncertain drag coefficient of the foundation
496 structures. This result is in line with a recent study by Christiansen et al. [19], despite the
497 idealised circular geometry of the OWF and the neglect of nonlinear effects. The model thus
498 provides theoretical guidance to understand the possible alteration of mean currents on the
499 continental shelves where OWFs are installed, or planned. The model is expected to apply
500 to shelf seas where there is no strong feedback between changes in bottom friction and tidal
501 currents, and in cases where the nonlinear terms are small. In future OWF scenarios where
502 larger farms are envisioned to be placed in deeper waters, the nonlinear terms are expected
503 to be less important.

504 The results show that reductions in mean currents are primarily a function of the ratio of
505 friction coefficients, q , between inside and outside the OWF, and scales similar to the linear
506 drag law result, i.e., with reduction $\sim q/(2 + q)$. This relation can be expressed directly in
507 terms of estimated OWF parameters as a reduction of $C_D^t/(4C_D^0\ell^2/A_f + C_D^t)$ in the mean
508 currents, with dependence on both the drag coefficients (structure and sea bed) and the
509 area ratio of the OWF structures and their spacing. Typical values for the reductions in
510 current scenarios of OWF development show that the current reductions are likely less than
511 10%, and show large variability depending on the density and geometry of the structures in
512 individual OWFs, where current reductions can also be negligible. Additional dependence
513 on the tidal ellipse parameters is also found, and can amount to deviations from this scaling
514 of more than 10%, especially at low q . In addition to a current reduction, there may also
515 be a deflection of the current inside the OWF, however, these angles of deflection are small
516 ($< 1^\circ$) for expected levels of q , with theoretical maximum deflections of $< 10^\circ$ for large q .

517 With our focus on a purely circular OWF geometry we have neglected to include a
518 parameter that describes a *farm* orientation. Such a parameter should have an effect on the
519 current field. In particular, we note that many OWF installations and development plans
520 have a polygon shape which may be possible to develop numerical solutions for using the
521 model derived herein. This is left for potential future work, which should also focus on the

522 influence of the nonlinearity parameter. We recommend conducting intermediate studies,
 523 between the idealised model presented herein and the realistic simulations of Christiansen et
 524 al.[19], that focus on the response of OWFs with realistic geometries and nonlinear effects.

525 ACKNOWLEDGMENTS

526 Support of JRC by the Helmholtz Association through the PoF-IV programme is grate-
 527 fully acknowledged. We also thank Nils Christiansen for his comments and support in
 528 quantifying North Sea tidal currents.

529 Appendix A. Derivation of the jump condition

530 As described above, the second jump condition that must be applied is derived by inte-
 531 grating the full equation $\hat{k} \cdot (\vec{\nabla} \times \mathbf{K}\vec{u}) = 0$, across the OWF boundary, where gradients of
 532 $c(x, y)$ are singular with delta function behaviour. In terms of the stream function, we write
 533 this as

$$534 \quad c\vec{\nabla} \cdot (\mathbf{k}^*\vec{\nabla}\psi) + \vec{\nabla}c \cdot (\mathbf{k}^*\vec{\nabla}\psi) = 0, \quad (65)$$

535 which correspond to the L_1 and L_2 operator terms in (9). Here we have defined

$$536 \quad \mathbf{k}^* \equiv \begin{bmatrix} -k_{yy} & k_{xy} \\ k_{xy} & -k_{xx} \end{bmatrix}. \quad (66)$$

537 These terms can be combined into

$$538 \quad \vec{\nabla} \cdot (c\mathbf{k}^*\vec{\nabla}\psi) = 0. \quad (67)$$

539 We then integrate this equation over some part of the domain, V , and apply the divergence
 540 theorem to show

$$541 \quad \int_V \vec{\nabla} \cdot (c\vec{A})dV = \int_{\partial V} c\vec{A} \cdot \hat{n}dS = 0, \quad (68)$$

542 where we denote $\vec{A} \equiv \mathbf{k}^*\vec{\nabla}\psi$, and \hat{n} the unit normal to the boundary ∂V . Since ∂V can
 543 be taken anywhere in the domain, we set it equal to the outside and inside of the OWF
 544 boundary, denoted Γ^\pm respectively. Then we can write

$$545 \quad \int_{\Gamma^+} c\vec{A} \cdot \hat{n}dS - \int_{\Gamma^-} c\vec{A} \cdot \hat{n}dS = 0 \quad (69)$$

546 so that taking the curves Γ^\pm infinitely close together leads to

$$547 \quad \llbracket c \vec{A} \cdot \hat{n} \rrbracket_\Gamma = 0, \quad (70)$$

548 and the general form for the jump condition of

$$549 \quad \llbracket c \mathbf{k}^* \vec{\nabla} \psi \cdot \hat{n} \rrbracket_\Gamma = 0. \quad (71)$$

550 This can alternatively be expressed in the form

$$551 \quad \llbracket c \mathbf{k} \vec{u} \cdot \hat{\tau} \rrbracket_\Gamma = 0, \quad (72)$$

552 where $\hat{\tau}$ is the unit tangent vector to the surface Γ . This form of the general jump condition
 553 in (72) has a simple physical interpretation, namely, that the tangential component of the
 554 frictional stress is continuous across the OWF boundary. This can be seen from the fact
 555 that the frictional stress is proportional to $c \mathbf{k} \vec{u}$ from (5).

556 We can verify that this general form produces the correct results in specific cases. In the
 557 case of linear friction with a circular OWF of radius R this becomes

$$558 \quad \llbracket c \psi_r \rrbracket_R = 0, \quad (73)$$

559 in agreement with [21].

560 For the same circular OWF where the friction is anisotropic, we can express

$$561 \quad (\mathbf{k}^* \vec{\nabla} \psi) \cdot \hat{n} = -k_{yy} \cos \theta \psi_x + k_{xy} \cos \theta \psi_y + k_{xy} \sin \theta \psi_x - k_{xx} \sin \theta \psi_y \quad (74)$$

562 and after switching to polar coordinates, this gives

$$563 \quad (\mathbf{k}^* \vec{\nabla} \psi) \cdot \hat{n} = -m \psi_r - n \frac{\psi_\theta}{r}. \quad (75)$$

564 Then accounting for the jump across $r = R$ we get the final form of the jump condition of

$$565 \quad m \llbracket c \psi_r \rrbracket_R - \frac{c t n}{R} \psi_\theta(R, \theta) = 0. \quad (76)$$

566 This form can alternatively be derived directly from (9) by substituting for the polar forms
 567 of the second derivatives and integrating across $r = R$ and using integration by parts.

568 **Appendix B. Derivation of $\beta = -\tilde{\theta}$**

569 Using the following identity

$$570 \quad \tan^{-1} x - \tan^{-1} y = \tan^{-1} \left(\frac{x - y}{1 - xy} \right) \quad (77)$$

571 we can write

$$572 \quad 2\beta = \alpha_+ - \alpha_- = \tan^{-1} \left(\frac{-2a}{a^2 + b^2 - 1} \right) \quad (78)$$

573 then we will substitute in for a, b using their definitions in terms of the \mathbf{k} components. It
574 is helpful to explicitly write the tensor components in terms of the tidal current ellipse
575 orientation via

$$576 \quad k_{xx} = \tilde{u}[g_1 - g_2 \sin^2(\tilde{\theta})] \quad (79)$$

$$578 \quad k_{yy} = \tilde{u}[g_1 - g_2 \cos^2(\tilde{\theta})] \quad (80)$$

$$580 \quad k_{xy} = \tilde{u} \frac{g_2}{2} \sin(2\tilde{\theta}) \quad (81)$$

581 with the coefficients g_i independent of $\tilde{\theta}$, and given by

$$582 \quad g_0 \equiv \left\langle \frac{\cos^2(\omega t)}{[\cos^2(\omega t) + \tilde{b}^2 \sin^2(\omega t)]^{1/2}} \right\rangle, \quad g_1 = 3g_0 - g_2, \quad g_2 \equiv \left\langle \frac{\cos^2(\omega t) - \tilde{b}^2 \sin^2(\omega t)}{[\cos^2(\omega t) + \tilde{b}^2 \sin^2(\omega t)]^{1/2}} \right\rangle. \quad (82)$$

583 Then, substituting in (79-81) above leads to

$$584 \quad \frac{-2a}{a^2 + b^2 - 1} = \frac{-2k_{xy}}{k_{xx} - k_{yy}} = -\tan(2\tilde{\theta}). \quad (83)$$

585 After using the odd property of the inverse tangent function, this gives the desired result of
586 $\beta = (\alpha_+ - \alpha_-)/2 = -\tilde{\theta}$.

587 **Appendix C. Solving the jump condition for τ**

588 The procedure that we use to solve the second jump condition (57) for τ is as follows.

589 It can be shown through substitution of the k_{ij} that

$$590 \quad m(\theta) = \tilde{u} \left\{ g_3 - \frac{g_2}{2} \cos[2(\theta - \tilde{\theta})] \right\} \quad \text{and} \quad n(\theta) = \tilde{u} \frac{g_2}{2} \sin[2(\theta - \tilde{\theta})] \quad (84)$$

591 where we have defined $g_3 \equiv g_1 - g_2/2$. It is important to note that the RHS can be expressed
592 as a purely sinusoidal function of θ (i.e. with unit frequency). This can be seen through the
593 results that

$$594 \quad m \cos \theta - n \sin \theta = \tilde{u} \left[g_3 \cos \theta - \frac{g_2}{2} \cos(\theta - 2\tilde{\theta}) \right] \quad (85)$$

595

596

$$m \sin \theta + n \cos \theta = \tilde{u} \left[g_3 \sin \theta + \frac{g_2}{2} \sin(\theta - 2\tilde{\theta}) \right], \quad (86)$$

597

combined with the fact that $\psi_{x,y}^0$ are constants. ψ^0 is the stream function of a uniform flow,

598

given by

599

$$\psi_0(x, y) = U(y \cos \lambda_0 - x \sin \lambda_0) - \frac{2\nu}{\rho} \text{Im}\{\tau e^{-i\phi} \xi\} \quad (87)$$

600

It can be expanded to give the gradients in the z -plane of

601

$$\psi_x^0 = -U \sin \lambda_0 - \tau_* \frac{2\nu}{\rho} [a \cos(\theta_* - \phi) + b \sin(\theta_* - \phi)] \quad (88)$$

602

603

$$\psi_y^0 = U \cos \lambda_0 - \tau_* \frac{2\nu}{\rho} \cos(\theta_* - \phi), \quad (89)$$

604

where we have defined $\tau \equiv \tau_* e^{i\theta_*}$.

605

Looking at the LHS, it is useful to multiply top and bottom of (61) by the complex

606

conjugate of the denominator and evaluate on the boundary (where $\chi\bar{\chi} = 1$) to get

607

$$\frac{d\Omega_1}{d\xi} = \frac{2\nu}{\rho e^{i\phi}} \cdot \frac{\nu(\tau/\nu + \bar{\tau}\nu - \overline{\tau\chi^2}/\nu - \nu\tau\chi^2)}{2\nu^2(\frac{1+\nu^4}{2\nu^2} - \cos[2(\theta - \tilde{\theta})])}. \quad (90)$$

608

But we can show that

609

$$\frac{1 + \nu^4}{2\nu^2} = \frac{2g_1 - g_2}{g_2} \equiv g_4 \quad (91)$$

610

so that

611

$$\frac{1 + \nu^4}{2\nu^2} - \cos[2(\theta - \tilde{\theta})] = \frac{2m}{\tilde{u}g_2}, \quad (92)$$

612

and finally we have

613

$$\frac{d\Omega_1}{d\xi} = \frac{g_2 \tilde{u}}{2\rho m} e^{-i\phi} \left(\frac{\tau}{\nu} + \bar{\tau}\nu - \frac{\overline{\tau\chi^2}}{\nu} - \nu\tau\chi^2 \right). \quad (93)$$

614

Substituting the above forms into the jump condition give us a LHS of

615

$$b \cos \theta \text{Im}\{e^{-i\phi} f\} + (a \cos \theta + \sin \theta) \text{Re}\{e^{-i\phi} f\} \quad (94)$$

616

where we have defined $f(\theta) \equiv \tau/\nu + \bar{\tau}\nu - \overline{\tau\chi^2}/\nu - \nu\tau\chi^2$, with $\chi = e^{i(\theta - \tilde{\theta})}$. The RHS can be

617

expressed as

618

$$\rho q \left\{ \left[\frac{2g_3}{g_2} \cos \theta - \cos(\theta - 2\tilde{\theta}) \right] \psi_x^0 + \left[\frac{2g_3}{g_2} \sin \theta + \sin(\theta - 2\tilde{\theta}) \right] \psi_y^0 \right\}. \quad (95)$$

619

This equation can now be used to solve for τ , by moving the terms on the RHS that are

620

proportional to τ to the LHS, giving a RHS independent of τ , and noting that the unknown

621

phase, θ_* , is independent of the amplitude, τ_* . We therefore first solve for θ_* by minimising

622 the mean absolute error between LHS and RHS for a range of θ_* . This is followed by a
623 similar optimisation procedure for τ_* .

-
- 624 [1] IEA, *Offshore Wind Outlook 2019*, Tech. Rep. (International Energy Agency, 2019).
- 625 [2] IEA, *Renewable Energy Market Update 2023*, Tech. Rep. (International Energy Agency, 2023).
- 626 [3] D.-G. f. E. European Commission, *Offshore renewable energy strategy*, Tech. Rep. (Publica-
627 tions Office of the European Union, 2020).
- 628 [4] J. van Berkel, H. Burchard, A. Christensen, L. O. Mortensen, O. S. Petersen, and F. Thomsen,
629 The effects of offshore wind farms on hydrodynamics and implications for fishes, *Oceanogr.*
630 **33**, 108 (2020).
- 631 [5] R. Dorrell, C. Lloyd, B. Lincoln, T. Rippeth, J. Taylor, C. Caulfield, J. Sharples, J. Polton,
632 B. Scannell, D. Greaves, R. Hall, and J. Simpson, Anthropogenic mixing in seasonally stratified
633 shelf seas by offshore wind farm infrastructure, *Front. Mar. Sci.* **9**, 10.3389/fmars.2022.830927
634 (2022).
- 635 [6] T. Miles, S. Murphy, J. Kohut, S. Borsetti, and D. Munroe, Offshore wind energy and the
636 Mid-Atlantic cold pool: a review of potential interactions, *Mar. Technol. Soc. J.* **55**, 72 (2021).
- 637 [7] K. Slavik, C. Lemmen, O. Kerimoglu, K. Klingbeil, and K. Wirtz, The large-scale impact
638 of offshore wind farm structures on pelagic primary productivity in the southern North Sea,
639 *Hydrobiologia* **845**, 35 (2019).
- 640 [8] U. Daewel, N. Akhtar, N. Christiansen, and C. Schrum, Offshore wind farms are projected
641 to impact primary production and bottom water deoxygenation in the North Sea, *Commun.*
642 *Earth Environ.* **3**, 10.1038/s43247-022-00625-0 (2022).
- 643 [9] National Academies of Sciences, Engineering, and Medicine, *Potential Hydrodynamic Impacts*
644 *of Offshore Wind Energy on Nantucket Shoals Regional Ecology: An Evaluation from Wind*
645 *to Whales* (The National Academies Press, Washington, DC, 2024).
- 646 [10] C. B. Hasager, P. Vincent, J. Badger, M. Badger, A. Di Bella, A. Peña, R. Husson, and P. J. H.
647 Volker, Using satellite sar to characterize the wind flow around offshore wind farms, *Energies*
648 **8**, 5413 (2015).
- 649 [11] A. Platis, S. Siedersleben, J. Bange, A. Lampert, K. Bärfuss, R. Hankers, B. Cañadillas,
650 R. Foreman, J. Schulz-Stellenfleth, B. Djath, T. Neumann, and S. Emeis, First in situ evidence

- 651 of wakes in the far field behind offshore wind farms, *Sci. Rep.* **8**, 10.1038/s41598-018-20389-y
652 (2018).
- 653 [12] N. Christiansen, U. Daewel, B. Djath, and C. Schrum, Emergence of large-scale hydro-
654 dynamic structures due to atmospheric offshore wind farm wakes, *Front. Mar. Sci.* **9**,
655 10.3389/fmars.2022.818501 (2022).
- 656 [13] H. Rennau, S. Schimmels, and H. Burchard, On the effect of structure-induced resistance and
657 mixing on inflows into the Baltic Sea: A numerical study, *Coastal Eng.* **60**, 53 (2012).
- 658 [14] J. Carpenter, L. Merckelbach, U. Callies, S. Clark, L. Gaslikova, and B. Baschek, Potential
659 impacts of offshore wind farms on North Sea stratification, *PLoS ONE* **11** (2016).
- 660 [15] L. Schultze, L. Merckelbach, J. Horstmann, S. Raasch, and J. Carpenter, Increased mixing
661 and turbulence in the wake of offshore wind farm foundations, *J. Geophys. Res. Oceans* **125**,
662 10.1029/2019JC015858 (2020).
- 663 [16] K. Raghukumar, T. Nelson, M. Jacox, G. Chang, L. Cheung, and J. Roberts, Projected cross-
664 shore changes in upwelling induced by offshore wind farm development along the California
665 coast, *Commun. Earth Environ.* **4**, 10.1038/s41598-018-20389-y (2018).
- 666 [17] L. Schultze, L. Merckelbach, and J. Carpenter, Turbulence and mixing in a shallow shelf sea
667 from underwater gliders, *J. Geophys. Res. Oceans* **122**, 10.1002/2017JC012872 (2017).
- 668 [18] J. Floeter, J. E. van Beusekom, D. Auch, U. Callies, J. Carpenter, T. Dudeck, S. Eberle,
669 A. Eckhardt, D. Gloe, K. Hänselmann, M. Hufnagl, S. Janßen, H. Lenhart, K. O. Möller,
670 R. P. North, T. Pohlmann, R. Riethmüller, S. Schulz, S. Spreizenbarth, A. Temming, B. Wal-
671 ter, O. Zielinski, and C. Möllmann, Pelagic effects of offshore wind farm foundations in the
672 stratified North Sea, *Prog. Oceanogr.* **156**, 154 (2017).
- 673 [19] N. Christiansen, J. Carpenter, U. Daewel, N. Suzuki, and C. Schrum, The large-scale impact
674 of anthropogenic mixing by offshore wind turbine foundations in the shallow North Sea, *Front.*
675 *Mar. Sci.* **10** (2023).
- 676 [20] P. Cazenave, R. Torres, and J. Allen, Unstructured grid modelling of offshore wind farm
677 impacts on seasonally stratified shelf seas, *Prog. Oceanogr.* **145**, 10.1016/j.pocean.2016.04.004
678 (2016).
- 679 [21] C. Garrett and P. Cummins, Maximum power from a turbine farm in shallow water, *J. Fluid*
680 *Mech.* **714**, 634 (2013).
- 681 [22] N. Heaps, Linearized vertically-integrated equations for residual circulation in coastal seas,

682 Dtsch. Hydrogr. Z. **31**, 147 (1978).

683 [23] O. Strack, *Analytical Groundwater Mechanics* (Cambridge University Press, 2017).